RSC Advances



This is an *Accepted Manuscript*, which has been through the Royal Society of Chemistry peer review process and has been accepted for publication.

Accepted Manuscripts are published online shortly after acceptance, before technical editing, formatting and proof reading. Using this free service, authors can make their results available to the community, in citable form, before we publish the edited article. This Accepted Manuscript will be replaced by the edited, formatted and paginated article as soon as this is available.

You can find more information about *Accepted Manuscripts* in the **Information for Authors**.

Please note that technical editing may introduce minor changes to the text and/or graphics, which may alter content. The journal's standard <u>Terms & Conditions</u> and the <u>Ethical guidelines</u> still apply. In no event shall the Royal Society of Chemistry be held responsible for any errors or omissions in this *Accepted Manuscript* or any consequences arising from the use of any information it contains.



Cite this: DOI: 10.1039/c0xx00000x

www.rsc.org/xxxxxx

ARTICLE TYPE

Novel SiO₂@Mg_xSi_vO_z composite with high-efficiency adsorption of **Rhodamine B in water**

Yanyan Pei a, Man Wang a, Qi Liu a, Xuefeng Xu a, Liangjie Yuan a*and Yu Zhao *

Received (in XXX, XXX) Xth XXXXXXXXX 20XX, Accepted Xth XXXXXXXXX 20XX 5 DOI: 10.1039/b000000x

A series of core-shell SiO₂@Mg_xSi_yO_z (SM) composites were synthesized with high efficiency for the adsorption of Rhodamine B (RhB). The composites were characterized by powder X-Ray Diffraction (XRD), Scanning Electron Microscopy (SEM), Transmission Electron Microscopy (TEM), nitrogen adsorption-desorption. The influences of different magnesium oxide addition, adsorbent dosage, 10 temperature, contact time and initial RhB concentration on RhB adsorption were investigated, and the optimized adsorption parameters were also obtained. The adsorption data was evaluated using Langmuir and Freundlich models, but high correlation coefficients (R²) confirmed the validity of Langmuir isotherm, with maximum adsorption capacity of 52.71mg/g at 313K. The kinetic data fitted pseudosecond order model well and thermodynamic studies showed that the adsorption process was spontaneous 15 and endothermic. Even after successive five cycles for the adsorption-desorption of RhB, the regenerated powders remained excellent adsorption capacity with more than 99% dye removal which could be utilized as an efficient and low-cost adsorbent for adsorption of RhB dye in wastewater.

Key words: SiO₂@Mg_xSi_xO₂composite; adsorption; rhodamine B; isotherms; kinetics

1. Introduction

20 Water is one of the most essential natural resources for human life and only 0.03% of the total water available on earth can be utilized for various human activities. However, increasing population growth and industrial booms have lead to serious water pollution especially the dyestuff pollution. Dye pollutants 25 produced by textile industries are becoming a major source of environmental contamination, above 1.6×10⁹m³ dye-containing wastewater per year drains into environmental water systems without treatment.2-4 Azo dyes such as Rhodamine B, methyl orange, orange II and so on occupy the main part of dye 30 pollutants and often become toxic to organisms. However, azo dyes in waste water are difficult to be removed, due to their complex composition and inert properties. So decolorization, mineralization and decomposition of azo dyes are still a challenge.6-8

35 For these reasons, several methods for removing dye pollution from waste water have been investigated, including coagulation, reaction, photo-degradation, chemical bio-degradation, ultrasound-degradation and reverse osmosis. These methods are often expensive and extremely sensitive to several experimental 40 conditions and in addition may cause undesirable secondary pollution. 10 While adsorption is considered to be more economic and eco-friendly for the removal of dyes from aqueous systems.¹¹ In recent years, extensive literature has been reported regarding dye removal from aqueous solutions by using a myriad of 45 adsorbents derived from clay minerals, 12 activated carbon, 13-15 coal,16 wood,17 carbon xerogels,18 fly ash,19-21 and biomaterials.^{22,23} Despite the fact that activated carbon is one of the most effective adsorbents, the use of activated carbon is an expensive process due to its high cost and difficulties in the 50 regeneration of adsorbed activated carbon. Therefore, the preparation of low-cost and recyclable adsorbent has become a focus to researchers for the last few years. 10, 24

In this paper, we synthesized a series of core-shell SiO₂@Mg_vSi_vO_z composites with high specific surface areas and 55 regular mesopores, which could be used as adsorbents in the removal of RhB from aqueous solution. Moreover, such adsorbent not only displayed higher adsorption capability and better desorption property, but also was easy to be regenerated. Herein, the micron-spherical SiO2 is chosen as the core material 60 for SiO₂@Mg_xSi_yO_z due to the following reasons.²⁵ Firstly, silica has a well-characterized surface and can be modified to a wide range of functionality owing to the presence of active hydroxyl groups. Secondly, silica surface is generally embedded with hydroxy groups and ethereal linkages, and hence considered to 65 have a negative charged surface prone to adsorption of electron deficient species. Furthermore, Silica is nontoxic to the environment and very stable due to its thermal stability and chemical inertness. In addition, Rhodamine B (RhB), a watersoluble organic dye widely used in textile industries for dyeing 70 cotton, wool, and silk, was selected as the model azo dye to evaluate the adsorption efficiency of SiO₂@Mg_xSi_vO_z. The system variables, adsorption isotherms, dynamics,

thermodynamics of adsorption were also investigated. The systematic and detailed investigation of SiO₂@Mg_xSi_yO_z materials prepared by facile and economic method was of great importance toward the application of removal of RhB dye from 5 aqueous solutions.

2. Experimental

2.1 Materials

The micron-sized silica spheres (D_{50} = 4.714 μ m) with a normal size distribution were obtained from Wuhan Shuaier Photo 10 Electronic Materials Corporation, Ltd., which were synthesized according to Ai's method.²⁶ Silica sol (25wt% of nano-SiO₂) was supplied by Wuhan Huanyu Chemical Corporation Ltd., magnesium carbonate basic pentahydrate $((MgCO_3)_4 \cdot Mg(OH)_2 \cdot 5H_2O,$ Rhodamine В (RhB) 15 purchased from Sinopharm Chemical Reagent Corporation, Ltd.. All the reagents were AR (analytical reagent) grade in purity and employed without purification. Deionized water was used in all the processes.

2.2 Preparation of SiO₂@Mg_xSi_vO_z

20 A series of SiO₂@Mg_xSi_vO_z (SM) materials were synthesized under ambient conditions with two procedures. First, the silica sol (25wt% of nano-SiO₂) was mixed with activated magnesium oxide in a mass ratio, then the micron-spherical SiO₂ was added into the mixture. The activated magnesium oxide was obtained 25 from magnesium carbonate basic pentahydrate by calcination at 650°C for 3h. Then the mixture was stirred in a mixing agitator with a speed of 1800rpm for 20min and then dried in an oven at 120°C for 6h. The dried solids were subsequently grinded, and calcined at 600°C for 3h in air. The obtained samples were named 30 as SM-X (X=1, 2, 3, 4, 5) according to the addition of activated MgO (wt%) at 10, 15, 20, 25 and 30%, respectively.

2.3 Characterization

XRD patterns of all the samples were obtained on a Bruker D8 advanced powder X-ray diffractometer using Cu Kα1 radiation 35 (λ =1.54060Å) at 40kV and 40mA. The powders were scanned from 10° to 80° (20) with a scan speed of 6° min⁻¹. The morphology of the samples was observed on a FEI Zeiss Sigma scanning electron microscopy (SEM). The internal structure of the samples was characterized by a JEOL JEM-40 100CX□ transmission electron microscope (TEM). X-ray photoelectron spectroscopy (XPS) was carried out on a Thermo Fisher ESCALAB 250Xi instrument with a monochromatic Al K Alpha (1486.68eV) X-ray source, and the binding energies were referenced to the C1s line at 284.8eV from 45 adventitious carbon. FT-IR spectra were collected by Fourier Transform Infrared Spectroscopy (Nicolet 5700) in the range of 500-4000cm⁻¹. N₂ adsorption-desorption isotherms were measured using Gemini

2390 at 77k. The specific surface areas were evaluated using Brunauer-Emmett-Teller (BET) method in 50 the p/p_0 range of 0.02-0.20. The pore size distributions were calculated using the Barrett-Joyner-Halenda (BJH) method based on the adsorption branch. The total pore volume was determined from the data at p/p₀=0.99. UV-vis adsorption spectra were recorded by UV-vis spectrophotometer (UV-vis, SHIMADZU ₅₅ UV-3600) from the scale range of 300-700nm.²⁷

2.4 Adsorption experiments

A stock solution of RhB (100mgL⁻¹) was prepared in deionized water, which was used to be diluted to obtain solutions of desired concentrations. Batch method was followed to carry out the 60 adsorption studies, which permitted the convenient evaluation of parameters that influence the adsorption process. The represent sample SM-5 (1.0g/L) was added to 50mL solution of RhB (10mg/L) taken in 250mL conical flasks. The solution was stirred in thermostatic water bath-cum-shaker at a constant speed of 65 120r/min at a given temperature. After equilibrium time had been reached, RhB solution was separated by centrifugation at 12000 rpm for 10min. The absorbance of clarified supernatant solution was collected by a UV-vis spectrophotometer.²⁸

The kinetic experiments were carried out with RhB solution (10-70 60mg/L) at three temperatures (293, 303 and 313K) as a function of equilibrium time in a similar manner. For contact time studies, the residual concentrations of RhB solution (5, 10, 20mg/L) with SM-5 (0.2g/L) were measured at varying time intervals between 10 and 420min. The pH of solution was 6.0-6.5 without 75 adjustment. The equilibrium concentration of RhB solution was calculated using the value of maximum absorbance obtained at wavelength (λ=554nm) from the UV-vis spectra. A calibration plot of RhB with known concentrations was prepared and used for calculation purpose. Adsorption efficiency or removal 80 percentage was calculated by Eq.(1) and the equilibrium adsorption capacity q_e (mg/g) was calculated using the Eq.(2)

$$Removal = \frac{c_0 - c_e}{c_0} \times 100\% \tag{1}$$

$$q_{\rm e} = \frac{(\mathsf{C}_0 - \mathsf{C}_{\rm e})V}{m} \tag{2}$$

Where C_o is the initial concentration of the RhB solution (mg/L), 85 C_e is the equilibrium concentration (mg/L), V is the volume of the RhB solution (mL), and m is the adsorbent mass (mg). Effects of different magnesium oxide addition, adsorbent dosage, temperature, contact time and initial RhB concentration on RhB adsorption by SM-5 were also investigated.

90 3. Results and discussion

3.1 XRD

Fig.1 shows the XRD patterns of SM-5 that before and after calcination respectively. The composites exhibit a broad peak at around 23° (20) attributed to the characteristic of amorphous SiO₂. 95 It could be seen that the composites before calcination exhibited two diffraction peaks at 2θ of 42.68, 62.26° of activated MgO. However, no distinct diffraction peaks were observed in calcinated composites indicated that the activated MgO was completely reacted with silica sol in the process of calcination. 100 The XRD spectra of other composites are shown in the supporting information (Fig.S1).

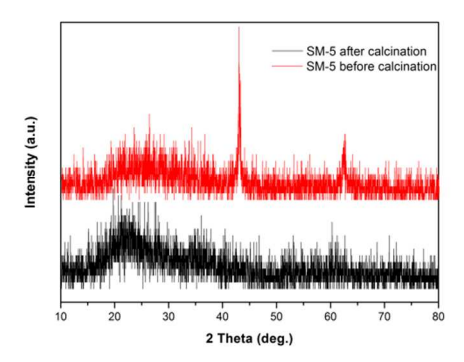


Fig.1 X-ray diffraction patterns of SM-5 before and after calcination.

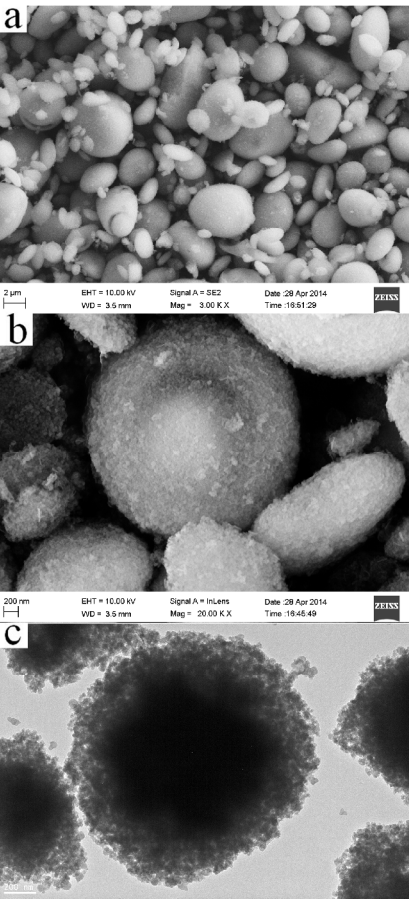


Fig.2 (a and b) SEM images of SM-5; (c) TEM image of SM-5.

5 3.2 SEM

The surface topography of the composite materials is obtained using SEM and two characteristic images of SM-5 are shown in Fig.2 (a and b). As shown in the SEM images, the morphology of SM-5 was approximately elliptical with the diameters of more 10 than 3µm. The surface of the particles was rough with many mesopores on the surface of SiO₂ spheres, indicating that silicon magnesium composites agglomerated on the external surface of the SiO₂ core, which could also be confirmed by nitrogen adsorption-desorption studies. It could be concluded that the 15 core-shell structure of SM-5 was formed with silicon magnesium oxides coated on the surface of SiO₂ micro-spheres. The morphologies of other composities were similar to SM-5 and the

SEM images are shown in the supporting information (Fig.S2).

3.3 TEM

20 The structural properties of SiO₂@Mg_xSi_vO_z materials were further investigated by transmission electron microscopy techniques. Fig.2(c) showed the TEM image of one representative sample SM-5 and illustrated that the micron-SiO2 was spherical which could be observed in the dark place, while the bright area 25 could be ascribed to the coated silicon magnesium oxides with different molecular formula. The TEM images further confirmed the core-shell structure of SiO₂@Mg_xSi_vO_z and the Mg_xSi_vO_z particles aggregated to form secondary particles that were tens of namometers in size, consistent with the results of XRD and SEM.

30 3.4 XPS

The surface composition, chemical status, and elemental content were further determined by means of XPS (Fig.3). XPS analyses indicate that the surface of composites contained the element of Mg, Si, O. The carbon peak is due to adventitious hydrocarbon 35 from the XPS instrument. In figure 3a, three individual peaks about 1304.76eV, 102.96eV, and 532.21eV could be evidently observed, which could be assigned to the binding energies of Mg 1s, Si 2p and O1s respectively. The high-resolution spectra of Mg 1s, Si 2p and O1s are shown in Fig 3(b, c and d). The calculated 40 surface atomic ratio of SM-5 for Mg, Si, O is 1:1.34:3.60. The atomic ratio of other composites are summarized in Table 1.

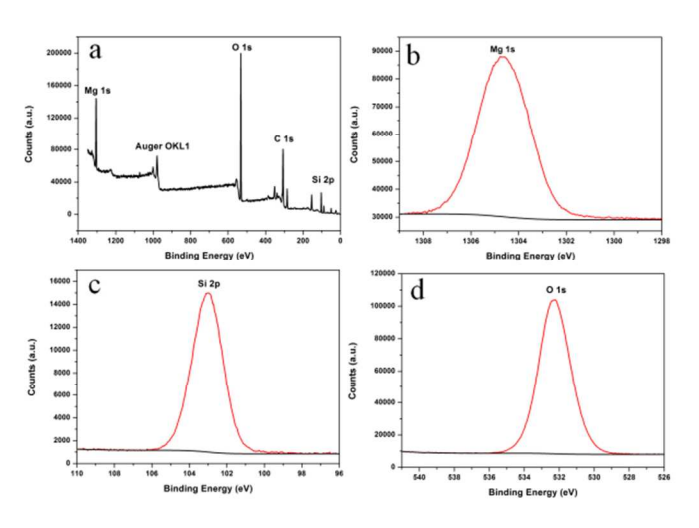


Fig.3 XPS spectra of SM-5: (a) survey scan; (b) Mg 1s; (c) Si 2p; (d) O 1s.

3.5 N₂ adsorption-desorption

45 The textural properties were investigated using nitrogen as the adsorption gas and the adsorption-desorption isotherms are depicted in Fig.4a. The isotherms showed a gradual increase in the amount of N2 adsorbed at low relative pressure values due to monolayer adsorption. As the relative pressure value increased, 50 multilayer adsorption occurred and this was followed by capillary condensation (the steep portion of the adsorption isotherm). The samples prepared in this study exhibited Type IV isotherms evidenced by a hysteresis loop which was the characteristic of mesoporosity. SM-4 and SM-5 showed H2 type hysteresis loops 55 which were characterized by a steep desorption branch. Such hysteresis loops had been attributed to the presence of ink bottle

pores with a narrow mouth (Fig.4a). However, SiO₂@Mg_xSi_vO_z materials with lower magnesium oxide addition, SM-1, SM-2 and SM-3 exhibited H3 type loops that were not leveled off at relative pressures that was very close to that of 5 saturation vapor pressure. Such loops were typical for materials that consisted of aggregates of plate-like particles forming slit like pores. As the addition of magnesium oxide further increased, the surface area increased and the results were summarized in Table 1.

10 The pore size distribution plots for corresponding samples are also showed in Fig.4b. As could be seen, the samples showed fairly narrow and unimodal pore size distribution with pores centered at near 3nm. It was found that there was no obvious difference among the five materials while the only difference was 15 the peak intensity. SM-4 and SM-5 had higher peak intensity, indicating more pores in comparison with the rest samples. This might be attributed to the higher amount of magnesium oxide which could form more pore structures on the surface of SiO₂ micro-spheres with the silica sol.¹¹

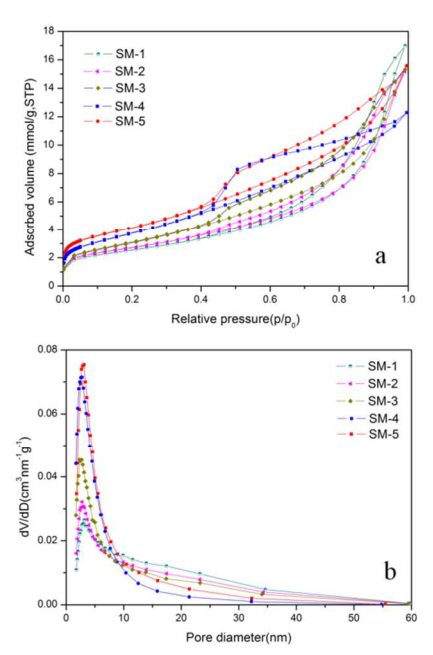


Fig.4 (a) Nitrogen isotherms and (b) pore size distribution of SM-1 to SM-5 with different magnesium oxide addition.

Table 1. Textural properties of various SiO₂@Mg_xSi_yO_z materials prepared by different addition of activated magnesium oxide

prepared by different addition of activated magnesiam oxide.					·.
Sample MgO		Chemical	SSA	PV(c	PD^b
	(wt%)	formula ^a	(m^2/g)	$m^3/g)$	(nm)
SM-1	10	$SiO_2@MgSi_{1.97}O_{4.58}$	204.55	0.59	3.18
SM-2	15	$SiO_2@MgSi_{1.92}O_{4.62}\\$	214.88	0.53	2.77
SM-3	20	$SiO_2@MgSi_{1.55}O_{3.97}$	249.85	0.53	2.34
SM-4	25	$SiO_2@MgSi_{1.41}O_{3.67}\\$	272.30	0.43	3.43
SM-5	30	$SiO_2@MgSi_{1.34}O_{3.60}\\$	311.00	0.54	3.11

²⁵ SSA, PV, and PD refer to specific surface area, pore volume, and pore diameter respectively

3.6 Adsorption studies

30 3.6.1 Effect of different magnesium oxide addition

The removal percentage of RhB adsorbed onto the five materials was in the following order: SM5 > SM4 > SM3 > SM2 > SM1(Fig.5a). This was consistent with the changing trend of BET surface area. Taking into account the efficiency of adsorption, 35 here our work mainly focused on the investigation of SM-5. It was noteworthy that most pores in SM-5 were larger than 3nm (Fig.4b), which were suitable to adsorb RhB as the length and width of RhB molecular were 1.8 and 0.7nm, ^{29, 30} respectively.

3.6.2 Effect of adsorbent dosage

40 To evaluate the adsorption efficiency of SM-5 for RhB, the dosage of SM-5 varied from 0.2 to 1.2g/L. The removal efficiency of RhB increased rapidly with the increase of adsorbent dosage (Fig.5b). This might be attributed to an increased adsorbent surface area and availability of more 45 adsorption sites. 31 Generally, adsorption reached saturated at dose of 1.0g/L and the dye uptake had a negligible decrease beyond 1.0g/L.

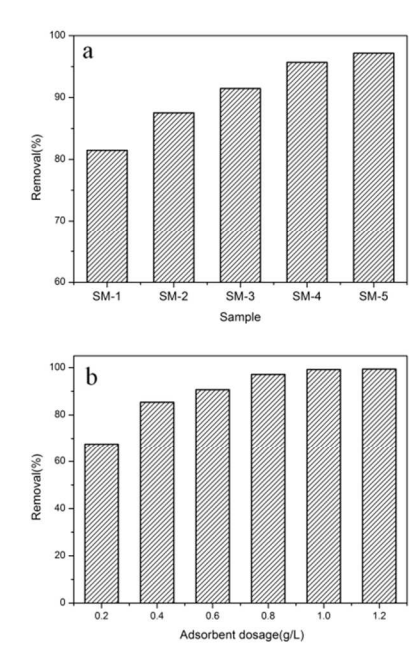


Fig.5 (a) Effect of different magnesium oxide addition on adsorption of RhB; 50 (b) effect of adsorbent dosage on adsorption of RhB by SM-5.

3.6.3 Effect of temperature

The adsorption of RhB onto SM-5 at 293, 303 and 313K (Fig.6a) indicated that the adsorption capacity increased with temperature from 293K to 313K and the adsorption was endothermic. This 55 phenomenon might be ascribed to these reasons: (a) increase in the rate of diffusion of adsorbate molecules across the external boundary layer and internal pores of the adsorbent, (b) an increase in the porosity and in the total pore volume of the adsorbent with temperature, (c) increase in the available active 60 sites for adsorption. 31, 32 Although adsorption was highest at 313K, all further experiments were carried out at 298K as most water resources had this temperature.

3.6.4 Effect of contact time and initial RhB concentration

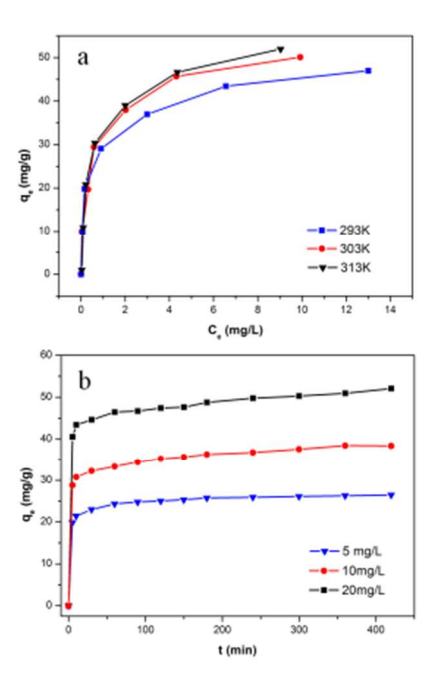
The adsorption capacity with corresponding contact time is also 65 shown in Fig.6b. The adsorption capacity increased with

^a Calculated from the atomic ratio of XPS spectra

^b Calculated from the adsorption branch of the isotherm

increasing contact time and reached equilibrium at around 5h. It was observed that dve uptake was rapid at the beginning, because of the availability of active sites and the high concentration gradient of RhB between the active sites and the aqueous solution. 5 And then, the rate of adsorption slowed down with decrease of available adsorption sites, during this process, the RhB molecules had to traverse deeper pores inside the particles and overcome a larger resistance. Moreover, high concentration required longer contact time to attain equilibrium because of the higher amount of 10 dye molecules. 36

Fig.6b also shows the effect of initial RhB concentration (5, 10, 20mg/L) on the adsorption of RhB at 298K. The equilibrium adsorption capacity increased from 24.78 to 52.05mg/g when the concentration of RhB increased from 5 to 20mg/L. This trend 15 could be ascribed to that a high concentration of RhB provided necessary driving force to overcome the mass transfer resistances between aqueous and solid phases, resulting in better adsorption of RhB onto SM-5 at a higher dye concentration.³



20 Fig.6 (a) Effect of temperature on adsorption of RhB by SM-5 (Conditions: Co, 10-60mg/L; adsorbent dose, 1.0g/L; temperature, 298k and pH, 6.0-6.5); (b) effect of contact time and initial RhB concentration on adsorption of RhB by SM-5 (Conditions: Co, 5,10,20mg/L; adsorbent dose, 0.2g/L and temperature, 298k and pH,6.0-6.5)

25 3.7 Mechanism of adsorption

The mechanism of adsorption could be explained by the chemical interactions between the dye molecules and the adsorbent. Chemical interactions include electrostatic attraction, covalent bonding, nonpolar interaction, water bridging, and 30 hydrogen-type bonding. Electrostatic interaction forces between dye molecules and the adsorbent structure are clearly involved because the dyes' molecules have a positive net charge and the adsorbent has a negatively charged surface (mainly due to hydroxyl groups on the surface).³⁷ In addition to electrostatic 35 interaction, there is the possibility of H-bond and water-bridge

formation between the amine, carboxylate, and heterocyclic N or O groups in the adsorbate organic structure and hydroxyl group. Hydroxyl groups are bonded to Si atoms at the Si-O-Si framework and as a consequence of the incomplete electronic Si 40 d layer, the electronic density distribution in the OH groups present a negative charge density highly displaced throughout the O atom. So a dipole is formed with the positive center located at the H atom. Moreover, dye molecules which have highly electronic displacements (peripheral dipoles, periphery 45 quadrupoles, and π -electronic clouds) could form H-bonds with the adsorbent surface. 38,39

FTIR analysis was carried out in order to identify the functional groups in the SM-5 that might be involved in the adsorption process. The FTIR spectrum of RhB is shown in 50 Fig.7a and the spectra of SM-5 before and after adsorption are shown in Fig.7b. The broad band positioned around 3430cm⁻¹ was assigned to the stretching vibration of hydroxyl functional groups. The broad peak located at 1091cm⁻¹ was attributed to asymmetric Si-O-Si vibrations; two peaks centered at 797 and 55 622cm⁻¹ due to symmetric Si-O-Si vibrations. The changes in peak frequency and intensity of FT-IR spectra before and after RhB adsorption suggested that Si-O-Si band and hydroxyl groups were involved in the adsorption process. The FTIR spectrum of SM-5 after adsorption revealed that many new peaks 60 were introduced into the spectrum after adsorption. These new peaks at 2800-3000 and 1300-1600cm⁻¹ were of significant intensities and corresponded to the peaks of RhB, indicating the adsorption of RhB molecules onto SM-5. The appearance of band at 1647cm⁻¹ could be assigned to the C=O of carboxylic 65 acids. The absorption bands around 1300-1600cm⁻¹ were assigned to aromatic skeletal vibration. The FTIR spectra suggest RhB might be adsorbed on SM-5 through hydrogen bond formation and π - π interaction.

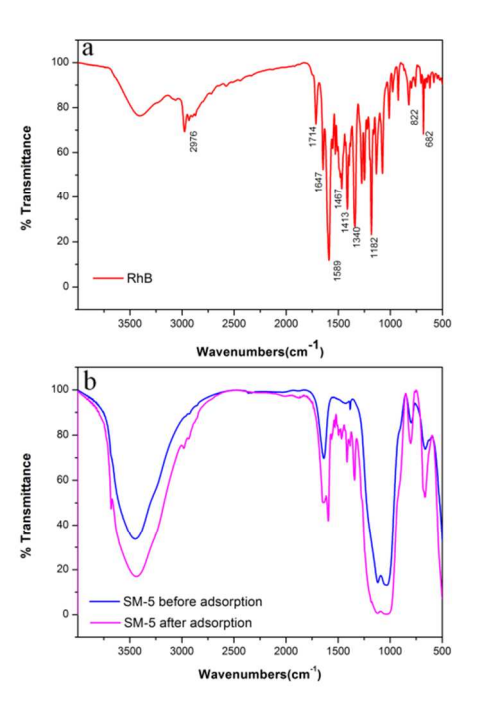


Fig.7 FT-IR spectra of (a) RhB and (b) SM-5 before and after adsorption.

3.8 Adsorption isotherm

The adsorption isotherm indicates how the dye molecules are distributed between the liquid phase and solid phase when the adsorption process reaches equilibrium. Two important isotherms, 5 the Langmuir isotherm and Freundlich isotherm are tested in this

Langmuir isotherm is valid for monolayer. The linearized form of equation is expressed as Eq.(3) (Langmuir,1918):

$$\frac{C_e}{q_e} = \frac{1}{bq_m} + \frac{C_e}{q_m} \tag{3}$$

Where C_e and q_e are the equilibrium liquid-phase and solid-phase 10 of concentration respectively; q_m (mg/g) is the monolayer capacity of the adsorbent; and b (L/mg) is the Langmuir adsorption constant, which is related to the adsorption energy. As shown in Fig.8a, the plots of C_e/q_e versus C_e at different temperatures (293, 303 and 313K) are linear, which indicated that 15 the adsorption data followed the Langmuir isotherm model.

The Freundlich isotherm is described by the following Eq.(4) (Freundlich, 1906):

$$\log q_e = \log K_F + \frac{1}{n} \log C_e \tag{4}$$

Where $K_{\rm F}$ (L/g) and n are the Freundlich constants of the system, indicators of adsorption capacity and adsorption intensity, 20 respectively, which are obtained from the slope and the intercept of the lineralized Freundlich plots (Fig.8b).

The results of Langmuir and Freundlich parameters at different temperatures are shown in Table 2. It could be concluded that the correlation coefficient (R^2) for Langmuir isotherm model was $_{25}$ higher than 0.99, and q_m calculated from the model was close to the experimental data. It illustrated that the Freundlich isotherm did not fit well with the equilibrium data while the adsorption of SM-5 could be well described by the Langmuir isotherm. In

addition, the adsorption capacity increased with the temperature 30 and the maximum adsorption capacity was 52.71mg/g at 313K, which was higher than most other adsorbents reported earlier (Table 3) for RhB adsorption. 40-42

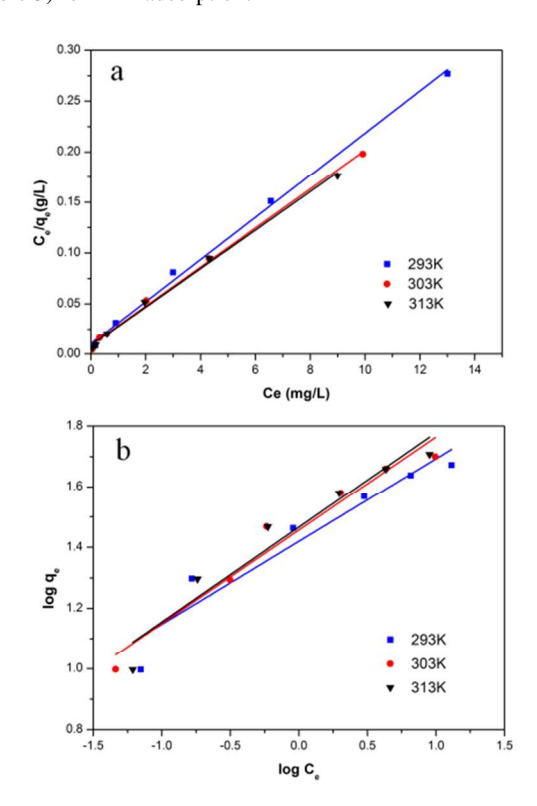


Fig.8 (a) Langmuir adsorption isotherm and (b) Freundlich isotherm plots for 35 adsorption of RhB onto SM-5.

Table 2. Isotherm parameters for adsorption of RhB onto SM-5

Temperature(K)	perature(K) Experimental Langmuir model			Freundlich model			
	$q_{max}(mg/g)$	$q_m(\text{mg/g})$	b(L/mg)	R^2	$K_F(L/g)$	n	R^2
293	49.26	48.10	1.99	0.9964	26.28	3.67	0.9006
303	52.34	51.98	2.08	0.9969	28.63	3.25	0.9491
313	55.06	52.71	2.17	0.9955	29.29	3.21	0.9263

Table 3. Comparison of adsorption capacity for adsorption of RhB with other adsorbents

Adsorbent	$q_m(\text{mg/g})$	Reference
Fly ash	10.0	Chang et al.(2009)
Modified parthenium biomass	18.5	Lata, Garg, and Gupt (2008)
Kaolinite	46.08	Khan, Dahiya, and Ali (2012)
Duolite C-20 resin	28.57	Al-Rashed and Al-Gaid (2012)
Hypercross-linked polymeric adsorbent	2.1	Huang et al.(2008)
Surfactant-modified coconut coir pitch	14.9	Sureshkumar and Namasivayam (2008)
Sago waste derived activated carbon	16.1	Kadirvelu et al.(2005)
Carbonaceous adsorbent	91.1	Bhatnagar and Jain (2005)
Used black tea leaves	53.2	Hossain et al.(2012)
SM-5	52.71	This work

Cite this: DOI: 10.1039/c0xx00000x

www.rsc.org/xxxxxx

ARTICLE TYPE

3.9 Adsorption kinetic studies

Adsorption kinetics of RhB, including the adsorption mechanism and rate controlling steps, were tested by pseudo-first order, pseudo-second order and intra-particle diffusion model.

5 3.9.1 Pseudo-first order model

The linear form of Pseudo-first order equation is given as Eq (5):

$$\log(q_{e} - q_{t}) = \log q_{e} - \frac{k_{1}t}{2.303}$$
 (5)

Where q_e (mg g⁻¹) and q_t (mg g⁻¹) are the adsorption capacity of RhB at equilibrium and at time t, respectively. k_l (min⁻¹) is the pseudo-first order rate constant. Values of k_l and q_e can be obtained from the slope and the intercept of the plot of $\log (q_e - q_t)$ versus t (Fig.9a).

3.9.2 Pseudo-second order model

The pseudo-second order model is expressed as Eq (6)

$$\frac{t}{q_{t}} = \frac{1}{k_{2}q_{e}^{2}} + \frac{t}{q_{e}} \tag{6}$$

Where k_2 (g/mg·min) is the pseudo second order rate constant. The intercept and slope of the plot of t/q_t and t provides the values of k_2 and q_e (Fig.9b).

The calculated values of correlation coefficients, adsorption capacities and rate constants are reported in Table 4. From the table we could see that the values of correlation coefficients 20 obtained from the pseudo second order (R²>0.99) were much better than the values obtained from the pseudo first order (R^2 = 0.9813 - 0.8491). Moreover, the calculated values of q_e by fitting pseudo second order model were almost same as the experimental values for all the concentrations studied, where as q_e values 25 obtained from pseudo first order model showed a larger deviation from the experimental values, which indicated that the adsorption process obeyed pseudo second order model well. In addition, the value of k_2 was found to decrease with increased initial dye concentration implying a higher diffusion rate of adsorption at 30 lower concentration. This may be attributed to the greater degree of distribution of dye over the surface of adsorbent for the adsorption process.

3.9.3 Intraparticle diffusion model

Adsorption involves three consecutive steps: liquid film ³⁵ diffusion, intraparticle diffusion and mass action. As mass action is very rapid and negligible for kinetic studies, the rate-limiting step is usually film diffusion or/and intra-particle diffusion. ⁴³

40 The Weber-Morris intraparticle diffusion model is applied to determine the rate-limiting step of adsorption process using the following expression:

$$q_t = k_i t^{0.5} + C$$
 (7)

Where k_i is the intraparticle diffusion rate constant (g/mg·min^{0.5}) and C is the constant that gives an idea about the thickness of the boundary layer. The plot of q_t vs. $t^{0.5}$ is shown in Fig.9c.

The adsorption process is controlled by the intraparticle diffusion model if the plot of q_t vs. $t^{0.5}$ gives a straight line and passes through the origin. Here, the plot of q_t vs. $t^{0.5}$ was a straight line but did not pass through the origin implied that the intraparticle diffusion was involved in the adsorption process but was not the only rate controlling step.²⁴

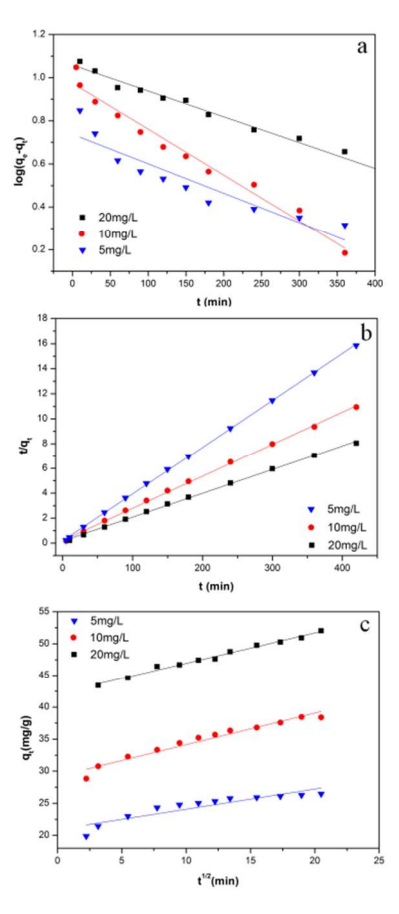


Fig.9 (a) Fit of kinetic data to pseudo first order model; (b) fit of kinetic data to pseudo second order model; (c) fit of kinetic data to intraparticle diffusion 55 mode.

Table 4. Kinetic parameters for adsorption of RhB onto SM-5.

Kinetic parameters	Initial concentrations(mg/L)			
remotic parameters	5	10	20	

$q_{e,exp}(\text{mg/g})$	24.78	38.40	52.05
Pseudo-first-order model			
$q_{e,cal}(ext{mg/g})$	4.98	9.44	11.13
$k_I(\min^{-1})$	0.0035	0.0048	0.0030
R^2	0.8491	0.9722	0.9813
Pseudo-second-order model			
$q_{e,cal}(\text{mg/g})$	26.60	38.76	52.08
$k_2(g/\text{mg}\cdot\text{min})$	0.0074	0.0032	0.0022
R^2	0.9998	0.9989	0.9988
Intra-particle diffusion model			
$k_i(\text{mg/g}\cdot\text{min}^{0.5})$	0.3148	0.4936	0.4763
C_{α}	20.94	29.21	42.17
R^2	0.8260	0.9528	0.9879

3.10 Adsorption thermodynamics

In order to fully understand the nature of the adsorption process, thermodynamic studies were performed. Thermodynamic parameters such as change in free energy (ΔG), enthalpy (ΔH) 5 and entropy (ΔS) were calculated using the following equations:

$$\Delta G = -RT \ln K_C \tag{8}$$

$$\ln K_C = \frac{-\Delta H}{RT} + \frac{\Delta S}{R} \tag{9}$$

Where K_C is the equilibrium constant, R is the gas constant (8.314) J·mol⁻¹k⁻¹) and T is the absolute temperature. The values of ΔH 10 and ΔS can be obtained from the slope and intercept of Van't Hoff plot of $ln K_C$ versus 1/T. The results are given in Table 5.

Table 5. Thermodynamic parameters of RhB adsorption by SM-5

Temperature	-ΔG	ΔΗ	ΔS	R^2
(K)	(kJ/mol)	(kJ/mol)	$(J/(k\!\cdot\!mol))$	
293	1.68	3.29	16.93	0.9999
303	1.84			
313	2.02			

 ΔG is a fundamental criterion to determine if a process occurs 15 spontaneously. The negative value of ΔG indicated the feasibility of the process and the spontaneous nature of the adsorption process. 44 Moreover, when the temperature increased from 293 to 313K, ΔG changed from -1.68 to -2.02kJ/mol, suggesting that adsorption was more spontaneous at higher temperature. The 20 positive value of ΔH (3.29kJ/mol) indicated that the process was endothermic in nature, which was also confirmed by the increased adsorption capacity of SM-5 for RhB with increasing temperature. In addition, the positive value of ΔS (16.93J·mol⁻¹k⁻¹) indicated an irregular increase of the randomness at the solid-25 liquid interface during the adsorption of RhB. 45,46

3.11 Desorption and recycling experiments

The most important requirement for the adsorbent is its reusability even after several adsorption-desorption cycles. This was tested by the constancy of its removal efficiency during the 30 repeated cycle. Initially, the spent samples saturated with RhB were filtered, dried then calcined at 600°C for 1h. The regenerated powder was used again for the next cycle of the adsorption of RhB. The adsorption -desorption experiments were carried on for the successive five cycles (Fig.10).

35 From Fig.10, adsorption efficiency was found to increase obviously compared with the initial adsorption for the next five cycles. The initial removal efficiency was 97.18% while after five

cycles it could reach 99.83%. This might be due to the increasing specific surface area of RhB calcinated and the adsorption sites 40 recovered from the regenerated samples. The results of N₂ adsorption and desorption are shown in Table 6, indicated that the specific surface area was indeed increased from 311.00 (Table 1) to 501.58m²/g. Such adsorbent not only possessed higher adsorption capability, but also showed better desorption property, 45 which could significantly reduce the overall cost for adsorbent. Therefore, it was suggested from the desorption studies that SiO₂@Mg_xSi_yO_z composites could be repeatedly used as an efficient adsorbent for the removal of RhB from contaminated water.

50 Table 6. Pore parameters of SM-5 regenerated by calcination with different repeat times.

SSA	PV	PD^{a}
(m^2/g)	(cm^3/g)	(nm)
357.88	0.42	3.06
458.96	0.51	3.38
434.43	0.55	3.39
470.73	0.59	3.36
501.58	0.66	3.35
	(m ² /g) 357.88 458.96 434.43 470.73	(m²/g) (cm³/g) 357.88 0.42 458.96 0.51 434.43 0.55 470.73 0.59

SSA, PV, and PD refer to specific surface area, pore volume, and pore diameter respectively

^a Calculated from the adsorption branch of the isotherm

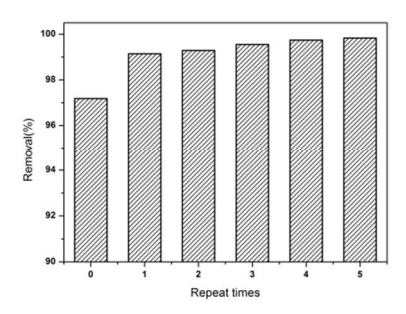


Fig. 10 Recycling experiment for adsorption of RhB onto SM-5 (Conditions: Co. 10mg/L; adsorbent dose, 1.0g/L; temperature, 298K and pH, 6.0-6.5).

4. Conclusions

A series of core-shell SiO₂@Mg_xSi_vO_z composites with high 60 efficiency for adsorption of Rhodamine B were successfully synthesized. The composition and structure of the composites were characterized by various analysis methods. The adsorption

process followed the Langmuir isotherm with maximum adsorption capacity of 52.71mg/g at 313K. Kinetic studies suggested that the adsorption mechanism fitted pseudo-second order model well and intraparticle diffusion was not the only rate 5 controlling step. Thermodynamic studies showed that the adsorption process was spontaneous and endothermic. The adsorbent showed very good reproducibility and reusability for the successive five cycles. Therefore, it concluded that SiO₂@Mg_xSi_yO_z composite can serve as a promising adsorbent 10 for practical use in the adsorption of pollutants.

Ackonwledgements

This work was supported by grants of the National Nature Science Foundation of China (No. 21471119), and large-scale Instrument and Equipment Sharing Foundation of Wuhan 15 University (No. LF20110063).

Notes and references

- ^a*College of Chemistry and Molecular Sciences, Wuhan University, Wuhan, China. Fax: +86-27-68754067; Tel: +86-27-68752800; E-mail: ljyuan@whu.edu.cn
- 20 **Analytical and Testing Center, Wuhan University, Wuhan, China. Fax: +86-27-68754067; Tel: +86-27-68752800; E-mail: icp@whu.edu.cn
 - † Electronic Supplementary Information (ESI) available: [details of any supplementary information available should be included here]. See DOI: 10.1039/b000000x/
- 25 1. H. Mittal and S. B. Mishra, Carbohydr. Polym. 2014, 101, 1255-1264.
- 2. O. J. Hao, H. Kim and P. C. Chiang, Crit. Rev. Environ. Sci. Technol. 2000, 30, (4), 449-505.
- 3. S. Eftekhari, A. H. Yangjeh and S. J. Sohrabnezhad, Hazard. Mater. 2010, 178, 349-355.
- 30 4. C. C. Chen, W. Zhao, J. Y. Li, Zhao, J. C. Zhao, H. Hidaka and N. Serpone, Environ. Sci. Technol. 2002, 36, 3604–3611.
- 5. N. Z. Bao, F. Xin, Z. H. Yang, L. M. Shen and X. H. Lu, Environ. Sci. Technol. 2004, 38, 2729-2736.
- 6. J. M. Joseph, H. O. Destaillats, H. Hung and M. R. Hoffmann, J. Phys. Chem. A. 2000, 104, 301-307.
- 7. C. J. G. Cornu, A. J. Colussi and M. R. Hoffmann, J. Phys. Chem. B. 2003, 107, 3156-3160.
- 8. K. P. Singh, D. Mohan, S. Sinha, G. S. Tondon and D. Gosh, Ind. Eng. Chem. Res. 2003, 42, 1965-1976.
- 40 9. T. A. Khan, M. Nazir and E. A. Khan, Toxicol. Environ. Chem. 2013, **95**, 919-931.
 - 10. M. A. Hossain and M. S. Alam, Iran J Environ Health Sci Eng. 2012, 9:2.
- 11. S. Rasalingam, R. Peng and R. T. Koodali, J. Environ. Manage. 2013, 128, 530-539.
- 12. T. A. Khan, V. V. Singh and D. Kumar, J. Sci. Res. 2004, 63, 355-
- 13. G. Annadurai, R. Juang and D. J. Lee, J. Environ. Sci. Health, Part A. 2001, **36**, 715-725.
- 50 14. C. Pelekani and V. L. Snoeyink, Carbon. 2000, 38, 1423-1436.
 - 15. S. Ramuthai, V. Nandhakumar, M. Thiruchelvi, S. Arivoli and V. Vijayakumaran, E-J. Chem. 2009, 6, S363-S373.
 - 16. S. V. Mohan, N. C. Rao and J. Karthikeyan, J. Hazard. Mater. 2002b, 90, 189-204.
- 55 17. V. K. Garg, R. Gupta, A. B. Yadav and R. Kumar, Bioresour. Technol. 2003. 89. 121-124.
 - 18. J. L. Figueiredo, J. P. S. Sousa, C. A. Orge, M. F. R. Pereira and J. J. M. Orfao, Adsorption. 2011, 17, 431-441.
- 19. J. X. Lin, S. L. Zhan, M. H. Fang, X. Q. Qian and H. Yang, J. Environ. Manage. 2008, 87, 193-200.
- 20. D. Mohan, K. P. Singh, G. Singh and K. Kumar, Ind. Eng. Chem. Res. 2002a, 41, 3688-3695.
- 21. W. Shaobin, Y. Boyjoo, A. Choueib and Z. H. Zhu, Water Res. 2005, 39, 129-138.

- 65 22. P. S. Guru and S. Dash, J. Dispersion Sci. Technol. 2013, 34, 898-907.
 - 23. S. Hii, S. Young and C. Wong, J. Appl. Phycol. 2009, 21, 625-631.
- 24. M. C. T. Largura, A. Debrassi, H. H. Santos, A. T. Marques and C. A. Rodrigues, Sep. Sci. Technol. 2010, 45, 1490-1498.
- 25. S. K. Parida, S. Dash, S. Patel and B. K. Mishra, Adv. Colloid Interface Sci. 2006, 121, 77-110.
- 26. C.C. Ai, Y. Xiao, W. Wen and L. J. Yuan, Powder Technol. 2011, **210**. 323-327.
- 27. L. X. Hu, F. Yang, W. C. Lu, Y. Hao and H. Yuan, Appl. Catal. B. 2013, 134-135, 7-18.
- 75 28. L.L. Ding, B. Zou, W. Gao, Q. Liu, Z. C. Wang, Y. P. Guo, X. F. Wang and Y. H. Liu, Colloids Surf. A. 2014, 446, 1-7.
- 29. H. M. H. Gad and A. A. El-Sayed, J. Hazard. Mater. 2009, 168, 1070-1081
- 30. Y. Guo, J. Zhao, H. Zhang, S. Yang, J. Qi, Z. Wang and H. Xu, Dyes Pigm. 2005, 66, 123-128.
- 31. T. A. Khan, S. Dahiya and I. Ali, Appl. Clay Sci. 2012, 69, 58-66
- 32. R. Srivastava and D. C. Rupainwar, Desalin. Water Treat. 2009, 11,
- 33. A. Ahmad, M. Rafatullah, O. Sulaiman, M. H. Ibrahim and R. Hashim, J. Hazard. Mater. 2009, 170, 357-365
- 34. J. Acharya, J. N. Sahu, B. K. Sahoo, C. R. Mohanty and B. C. Meikap, Chem. Eng. J. 2009, 150, 25-39.
- 35. I. A. W. Tan, A. L. Ahmad and B. H. Hameed, J. Hazard. Mater. 2008, 154, 337-346.
- 90 36. S. Senthilkumaar, P. R. Varadarajan, K. Porkodi and C.V. Subbhuraam, J. Coll. Interf. Sci. 2005, 284, 78–82.
- 37. P. V. Messina and P. C. Schulz, J. Coll. Interf. Sci. 2006, 299, 305-
- 38. S. Dash, S. Mishra, S. Patel, B. K. Mishra, Adv. Colloid Interface Sci. 2008, 140, 77-94.
- 39. S. K. Parida and B. K. Mishra, J. Coll. Interf. Sci. 1996, 182, 473-477.
- 40. L. Li, S. X. Liu and T. Zhu, J. Environ. Sci .2010, 22, 1273-1280.
- 41. Y. Yu, Y. Y. Zhuang and Z. H. Wang, J. Coll. Interf. Sci. 2001, 242, 288-293
- 100 42. J. Goel, K. Kadirvelu, C. Rajagopal and V. K. Garg, J. Hazard. Mat. 2005,125, 211-220.
 - 43. N. K. Lazaridis and D. D. Asouhidou, Water Res. 2003, 37, 2875-
- 44. R. Boopathy, S. Karthikeyan, A. B. Mandal and G. Sekaran, Environ Sci Pollut Res. 2013, 20, 533-542.
- 45. M. Ugurlu and M. H. Karaoglu, Micropor Mesopor Mater. 2011, **139**,173-178.
- 46. M. Ugurlu, A. Gurses and M. Acikyildiz, *Micropor Mesopor Mater*. 2008, 111,228-235.

Graphical abstract

A novel core-shell $SiO_2@Mg_xSi_yO_z$ composite were synthesized, which can be repeatedly used as an efficient adsorbent for the removal of RhB.

